

# We are IntechOpen, the world's leading publisher of Open Access books Built by scientists, for scientists

6,900

Open access books available

185,000

International authors and editors

200M

Downloads

Our authors are among the

154

Countries delivered to

TOP 1%

most cited scientists

12.2%

Contributors from top 500 universities



WEB OF SCIENCE™

Selection of our books indexed in the Book Citation Index  
in Web of Science™ Core Collection (BKCI)

Interested in publishing with us?  
Contact [book.department@intechopen.com](mailto:book.department@intechopen.com)

Numbers displayed above are based on latest data collected.  
For more information visit [www.intechopen.com](http://www.intechopen.com)



# Mammographic Quality Control Using Digital Image Processing Techniques

Mouloud Adel and Monique Rassigni

*Université Paul Cézanne, Institut Fresnel, UMR-CNRS 6133*

*Domaine Universitaire de Saint Jérôme,  
France*

## 1. Introduction

Breast cancer is the leading cause of cancer mortality among middle aged women. Survival and recovery depend on early diagnosis. At present mammography is one of the most reliable methods for early breast cancer detection. However relevance of diagnosis is highly correlated to image quality of the mammographic system. Hence periodic controls in mammographic facilities are necessary in order to make sure they work properly. In particular global image quality is evaluated from a mammographic phantom film. A phantom is an object with the same anatomic shape and radiological response as an average dense fleshed breast and in which are embedded structures that mimic clinically relevant features such as microcalcifications, nodules and fibrils. For each category of features, the targets have progressively smaller sizes and contrast so that the largest one is the most readily visible and the next is less visible and so on. Using a phantom makes it possible to free from the variable of differences in breast tissue positioning and level of compression from patient to patient. The process is as follows: the mammographic phantom film is analysed independently by several readers and a score is obtained by each of them depending on the number of objects they see. The independent object visibility scores are then averaged and the resulting score is assigned to the phantom film.

Automating this score by using computer image processing of digitized phantom films should make the evaluation of mammographic facilities easier and less subjective. In addition image processing should enable us to take into account other parameters such as, for instance, noise, texture and shape of the targets that a reader eye cannot estimate quantitatively, and so to perform a more elaborate analysis. In collaboration with ARCADES (Association pour la Recherche et le Dépistage des Cancers du Sein et du col de l'utérus) which set, since 1989, a breast cancer screening program in South of France, a project aimed at automating phantom film evaluation is in progress. Such a project consists first in digitizing phantom films with the adequate spatial resolution and then in processing the obtained images in order to detect, segment and characterize the objects contained in the phantom.

Little work has been done to automate quality control in mammographic facilities. Fast Fourier transform is used (Brooks et al., 1997) to establish some visibility criteria for the phantom test object. (Chakraborty et al., 1997) compares phantom images with a pattern image to obtain relations between some of the image parameters and the physical conditions

in which the images have been obtained. His work concerned only microcalcifications. (Dougherty, 1998) studies the most prominent microcalcification group and the most prominent mass using a manual threshold and some mathematical morphology operators. (Castellano et al., 1998) used binary masks to locate microcalcifications and they studied image resolution scales contained in the phantom. (Blot et al., 2003) used grey level co-occurrence matrices to score structures embedded in the phantom. (Mayo et al., 2004) used region growing and morphological operators to segment and characterize microcalcifications. They also studied horizontal resolution areas using morphological operators. This chapter presents a feasibility study aiming at automating phantom scoring using image processing techniques on digitized phantom films.

In the following sections, we describe the phantom used, the mammographic phantom image acquisition and digitization, the noise reduction and the contrast enhancement schemes used for processing phantom images, the segmentation step for each object (microcalcifications, masses and fibres) and the results obtained on nine phantoms films.

## **2. Description, acquisition and digitization of phantom films**

### **2.1 Phantom description**

The phantom used in this study is the MTM 100/R (Computerized Imaging Reference Systems, Inc., 2428 Alameda Avenue Suite 212, Norfolk, VA 23513, U.S.A., Phantom Serial Number: 2788). The MTM 100/R is used in France for Mammography Accreditation. It is made of tissue equivalent material in which are embedded objects simulating 7 pentagonal-shaped groups of microcalcifications (M1 to M7), 7 masses (N1 to N7) and 7 fibres (F1 to F7). For each category of features, the targets have progressively smaller size and contrast so that the largest one is the most readily visible, the next is less visible and so on. For convenience M1 stands for the microcalcification group containing the largest specks and M7, the smallest ones, with a similar convention for the other target structures. Inside are also present vertical (V) and horizontal (H) spatial resolution scales (line pair target : 20 lp/mm), a delimited zone (Z) for measuring a reference optical density, two different optical density contiguous areas (C1 and C2) for defining contrast, three cavities (D) for x-ray dose measurement and at last small balls (B) for x-ray alignment control. Figure 1 shows a schematic diagram of the MTM 100/R phantom.

### **2.2 Acquisition and digitization of phantom films**

Phantom films are digitized with an ultra high resolution drum scanner (Scanmate 11000-ScanView A/S.Meterbuen 6. DK-2740 Skovlunde. Denmark) which may digitize from 50 to 11000 dpi (dots per inch) and code images on 256 (8bits /pixel) or 16384 (14bits /pixel) grey levels. Spatial scanning resolution was chosen so that it approximately corresponds to the resolving power of a viewer (with a standard resolving power  $\sim 4.10^{-3}$ rd) using a twice magnifying lens (such lenses are often used by radiologists for reading clinical mammograms). So phantom films were digitized with a resolution of 50  $\mu$ m per pixel (or 508 dpi) and were coded on 256 grey levels.

For each category of structures (microcalcifications, masses and fibers) a sub-image was extracted from the digitized phantom image so that each sub-image contained one target and was roughly centered on it. Subimages sizes were 256×256-pixels for microcalcification groups and masses and 412×412-pixels for fibres. Fig. 2 shows an example of subimages extracted from a digitized phantom film.

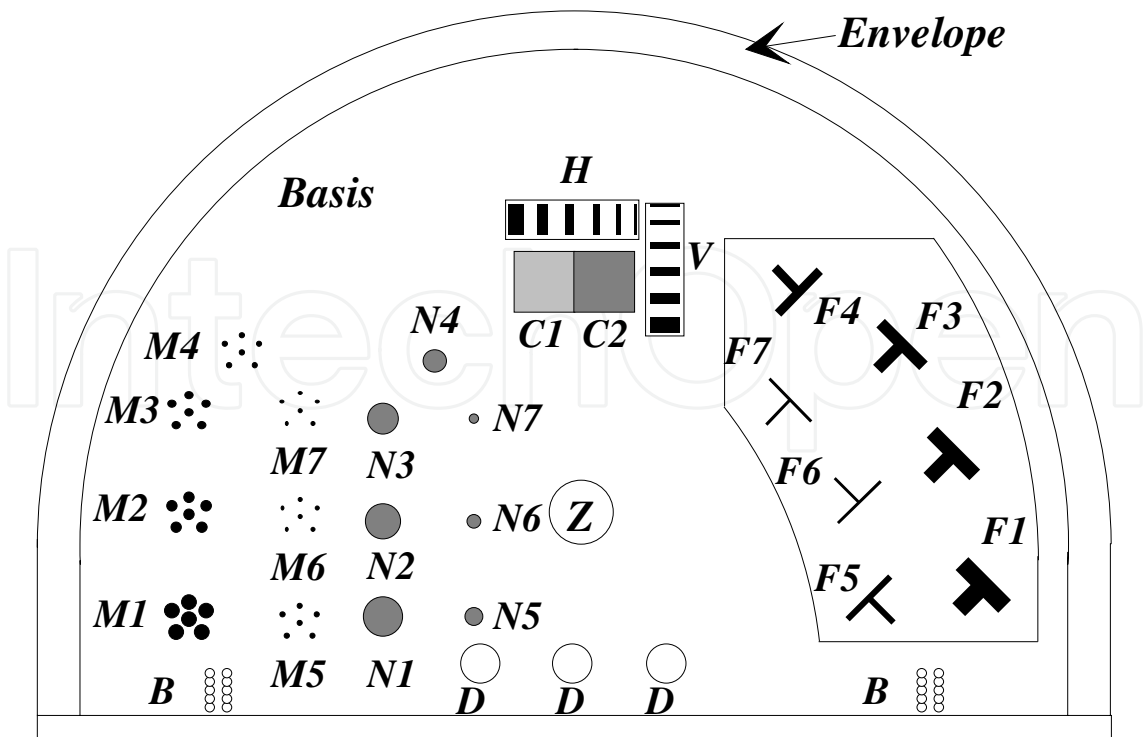


Fig. 1. Schematic diagram of the phantom MTM 100/R showing the locations and the relative size of features.

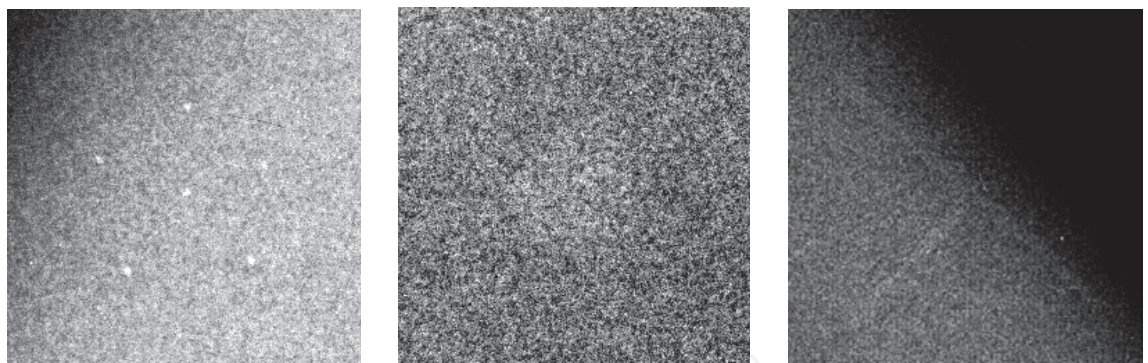


Fig. 2. Subimages extracted from a digitized phantom film. (a) : group of microcalcifications (b) : mass; (c) : fibre

3. Image processing of digitized phantom films

3.1 General description

Two pre-processing steps are applied to each extracted subimage before the segmentation step as shown in Fig. 3. Because of the noisy nature of these subimages, a noise reduction method is used as a first processing step. A contrast enhancement step is then applied. At last image segmentation is done.

3.2 Local contrast modification method description

In classical image processing techniques, a fixed shape and a fixed size window around each pixel is used in order to convolve it with a defined filter. In order to take the local features

around each pixel into account, a variable shape and size neighbourhood is defined (Dhawan et al., 1986; Dhawan & Le Royer, 1988) using local statistics. Noise reduction step consist in filtering two kinds of noise. The non uniform background considered as a "low frequency noise" and the radiographic noise (high frequency noise): film granularity and quantum mottle. Shadow correction of the background is adapted to each object (microcalcifications, masse and fibre), whereas the radiographic noise filter and the contrast enhancement steps are based on the same method, described in the next section. This method consists in computing a local contrast around each pixel using a variable neighbourhood whose size and shape depend on the statistical properties around the given pixel. The obtained image is then transformed into a new contrast image using various contrast modification functions. At last an inverse contrast transform is applied on the new contrast image to yield an enhanced version of the original image. Contrast enhancement step consists in enhancing image features while preserving details for the segmentation step. Image Segmentation is adapted to the objects to be detected and is presented in the following sections.

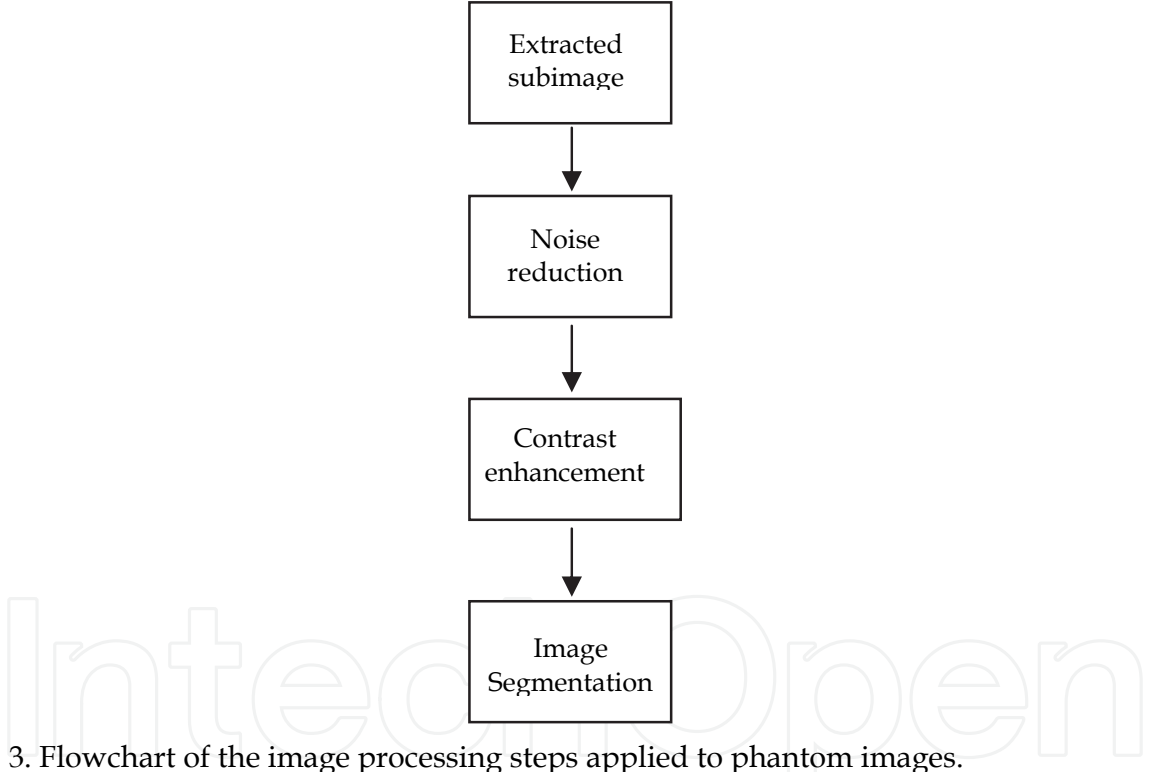


Fig. 3. Flowchart of the image processing steps applied to phantom images.

Each pixel  $(i,j)$  is assigned an upper window  $W_{max}$  centered on it, whose size is  $(2N_{max}+1) \times (2N_{max}+1)$ . We also define an inner area around the pixel  $(i,j)$  whose size is  $(c \times c)$  and an external area whose size is  $(c+2) \times (c+2)$ , where  $c$  is an odd number. Let  $I(i,j)$  be the grey level of pixel  $(i,j)$  in image  $I$ , and  $T$  a given threshold. Pixel  $(k,l)$  within  $W_{max}$  is assigned a binary mask value "0" if  $|I(k,l) - I(i,j)| > T$ , else it is assigned a binary mask value "1". Then the percentage  $P_0$  of zeros is computed over the region between the external  $(c+2) \times (c+2)$  and the inner  $(c \times c)$  areas, for each  $c$  in the range  $[1, 3, 5, \dots, 2N_{max} - 1]$ . The process stops if this percentage is greater than 60% or if the upper window  $W_{max}$  is reached. The value of 60% has been chosen because beyond this limit, we may consider too many pixels "0" are surrounding the inner area and so the notion of neighbourhood with the central pixel  $(i,j)$  in



terms of grey levels is no longer satisfactory. Let  $c_0$  be the upper  $c$  value beyond which the percentage  $P_0$  is greater than 60%. The pixel  $(i,j)$  is assigned the window  $W=(c_0+2)\times(c_0+2)$ . In the window  $W$  such as  $W\leq W_{max}$  we finally define the "center" as the set of pixels having the mask value "1", and the "background" as the set of pixels having both the mask value "0" and which are 8-neighbourhood connected at least to a pixel "1". Pixels "0" which do not verify the previous constraint belong neither to the "center" nor to the "background" and are not taken into account later on. Fig. 4 gives an example the way the "center" and the "background" areas are determined.

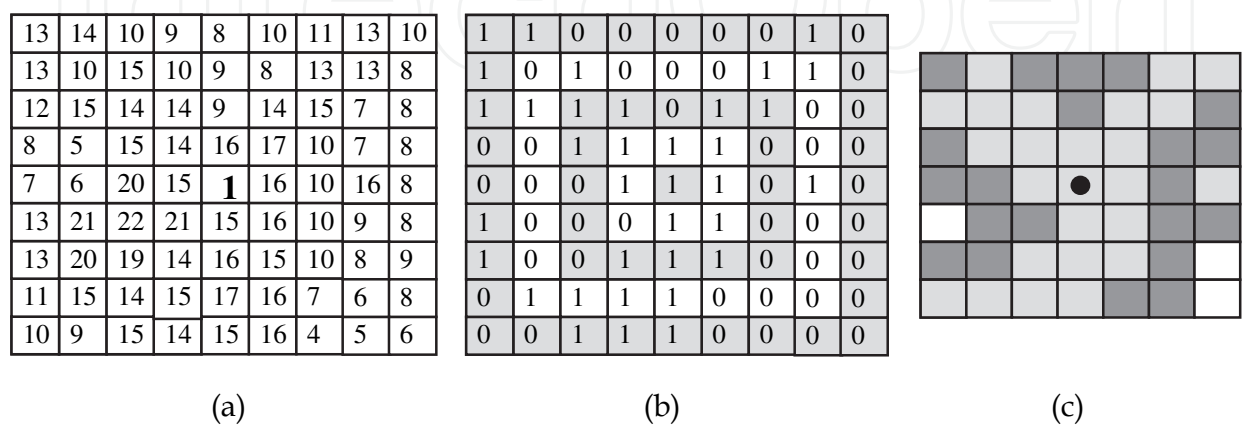


Fig. 4. Adaptive neighbourhood selection with a threshold value  $T=5$ ; (a)  $W_{max}$  window around bold-faced pixel value 15,  $N_{max}=4$ ; (b) Mask values associated to test pattern in (a); (c) The "center" (light grey) and the "background" (dark grey) areas around the bold-faced pixel. White cells correspond to pixels belonging neither to the "center" nor to the "background".

After determining the "center" and the "background" regions around each pixel  $(i,j)$ , a local contrast image  $C$  is computed from :

$$C(i,j)=\frac{|M_c(i,j)-M_b(i,j)|}{\max(M_c(i,j),M_b(i,j))} \tag{1}$$

where  $M_c(i,j)$  and  $M_b(i,j)$  are the mean values, in image  $I$ , of pixels labelled as the "center" and as the "background" regions around pixel  $(i,j)$  respectively. Note that  $C(i,j)$  is within the range  $[0,1]$ .

The local contrast image  $C$  obtained in the previous step is transformed into a new image  $C'$  such as  $C'(i,j)=\psi(C(i,j))$ , where  $\psi$  is a contrast modification function depending on features to be detected. This function meets some requirements in the interval  $[0,1]$  :

- $\psi(0) = 0$  and  $\psi(1) = 1$ .
- $\psi(x) \geq 0$  for  $x \in [0,1]$ .
- $\psi$  is an increasing function in the range  $[0,1]$ .

In image  $C'$  each pixel value is a contrast value. In order to obtain the corresponding image in the grey level domain, an inverse contrast transform of the process used to obtain image  $C$  from  $I$  (Eq. 1) is used as follows:

$$E(i,j)=M_b(i,j)(1-C'(i,j)) \text{ if } M_b(i,j) \geq M_c(i,j)$$

$$E(i, j) = \frac{M_b(i, j)}{(1 - C'(i, j))} \text{ if } M_b(i, j) < M_c(i, j)$$

This transform gives a new image E which is an enhanced version of image I. It is then possible to evaluate the efficiency of the method from comparison between images E and I.

### 3.2.1 Performance evaluation on simulated images

Several functions including square root, exponential, polynomial and trigonometric were tested (Guis et al., 2003). Actually functions which are over the line  $y=x$  increase the contrast but enhance the noise too. In the other hand, functions which are under the line  $y=x$  yield noise reduction. Because of the noisy nature of real images of phantom, the second kind of functions was chosen for enhancing the objects contained in these images. To choose suitable function  $\psi$ , computer simulated images containing objects similar to those observed in the phantom film were generated with various contrast and noise levels. The aim of this simulation was to perform a quantitative evaluation of the noise reduction method described in previous sections. For each target, 6 noise-free images were generated each of them with a different contrast level. Three noise levels were then assigned to each contrast level image. Contrast level is defined as the difference between the mean grey level of the object and the mean grey level of the background divided by the mean grey level of the background. According to studies on radiographic noise, two types of noise sources, namely film granularity and quantum mottle, are present in an X-ray image. Spatially correlated Poisson noise model has to be considered in the case of mammographic films. In our simulations, a signal-dependent spatially uncorrelated Gaussian noise is used as a first-order approximation of the Poisson noise model (Quian et al., 1994; Aghadasi et al., 1992; Kuan et al., 1985) namely:  $n(i, j) = \sqrt{f(i, j)}u(i, j)$ , where  $f$  is the noise free image and where  $u$  is a zero-mean Gaussian noise with standard deviation  $\sigma$ . The computer simulated image or noisy image  $g$  is then given by  $g(i, j) = f(i, j) + n(i, j)$ .

Contrast levels of noise free images were in the range [10%; 60%] with a step size of 10%. Background grey-level was set to 128. Concerning noisy images, standard deviation  $\sigma$  of the zero-mean Gaussian noise  $u$  was adjusted so that the signal to noise ratio (SNR) takes the values 21dB, 15dB and 9dB which simulate a low, an intermediate and a high noise level respectively. Computer simulated images consist of 256×256-pixels for microcalcification groups and nodules, and 336×336-pixels for fibres. The whole computer simulated images were coded on 256 grey levels.

Two criteria are used to test the effectiveness of the algorithm on computer simulated images. The first one, namely output to input Signal to Noise Ratio (SNR)  $\rho$ , quantifies noise suppression, and the second one, namely the mean-squared error (MSE), in addition to quantify noise removal gives also an information on structure distortion and therefore better interprets the first criterion. One can notice that parameter  $\rho$  is all the more higher as the method removes much more noise, whereas MSE parameter is all the smaller as the method denoises and preserves structures in the image.

Results obtained on simulated images show that the trigonometric function  $\psi(x) = \tan\left(\frac{\pi}{4}x\right)$  gives the best balance between noise reduction and edge sharpness preservation and that  $\psi(x) = \sqrt{x}$  is suitable for contrast enhancement.

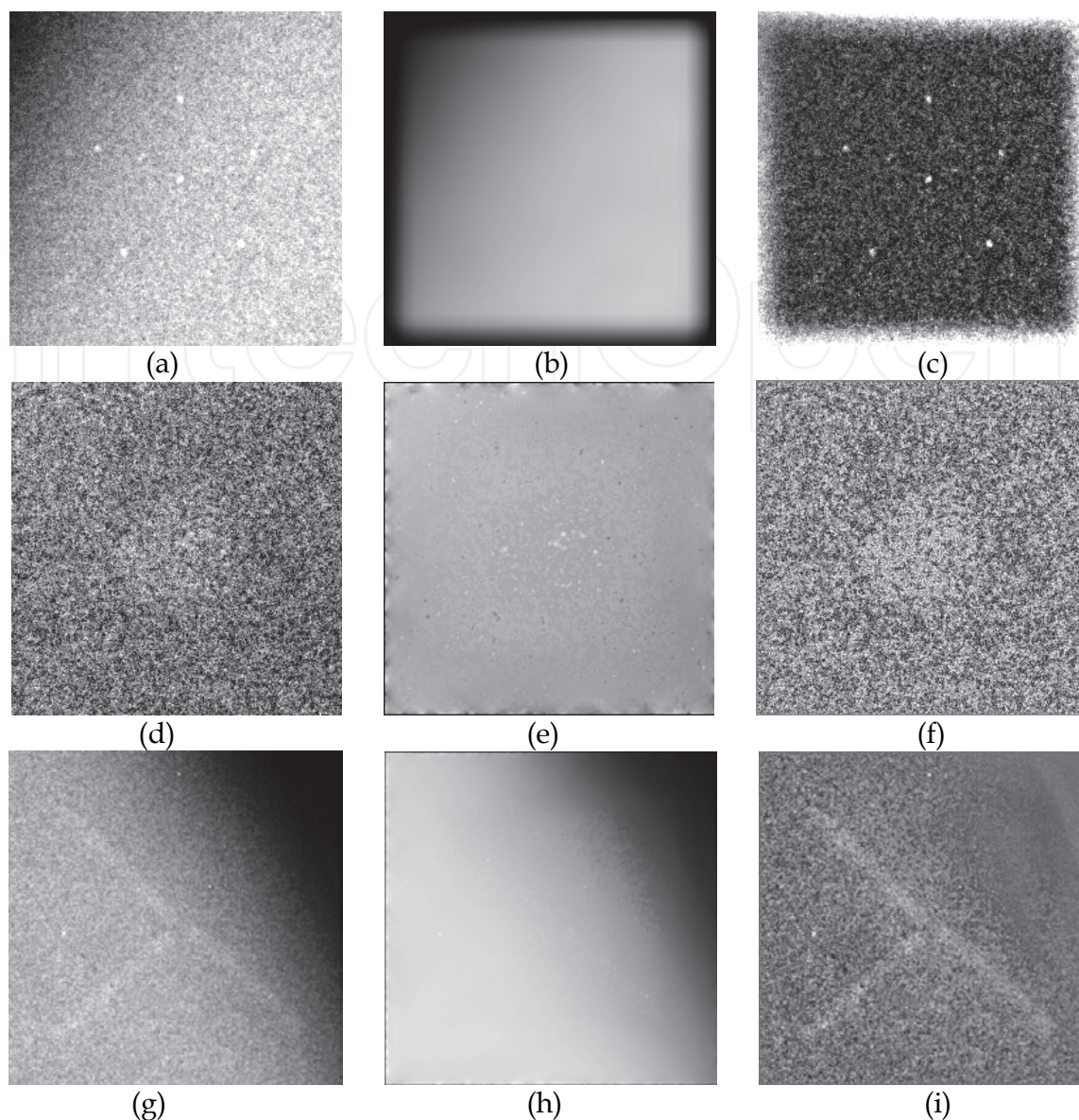


Fig. 5. Correction of Background inhomogeneity on extracted subimages. (a), (d) and (g) : original extracted subimages; (b), (e) and (h) background images; (c), (f) and (i) corrected images.

### 3.2.2 Preprocessing of real phantom images

Before applying noise reduction and contrast enhancement steps, inhomogeneous background of subimages containing microcalcification is extracted using the classical multiresolution Burt decomposition into level 3 (level 0 is the original image). A linear interpolation is then applied to obtain background image. The same method was not suitable to correct background for subimages containing masses and fibres, due to the object to image size ratio. Using the local contrast modification method described above with a big window size for  $W_{\max}$ , enabled us to obtain background image. At last corrected image for the whole objects is obtained by subtracting the background image from the original image as shown in Fig. 5.

Applying the noise reduction and contrast enhancement steps described in the previous section, yield the images shown in Fig. 6.



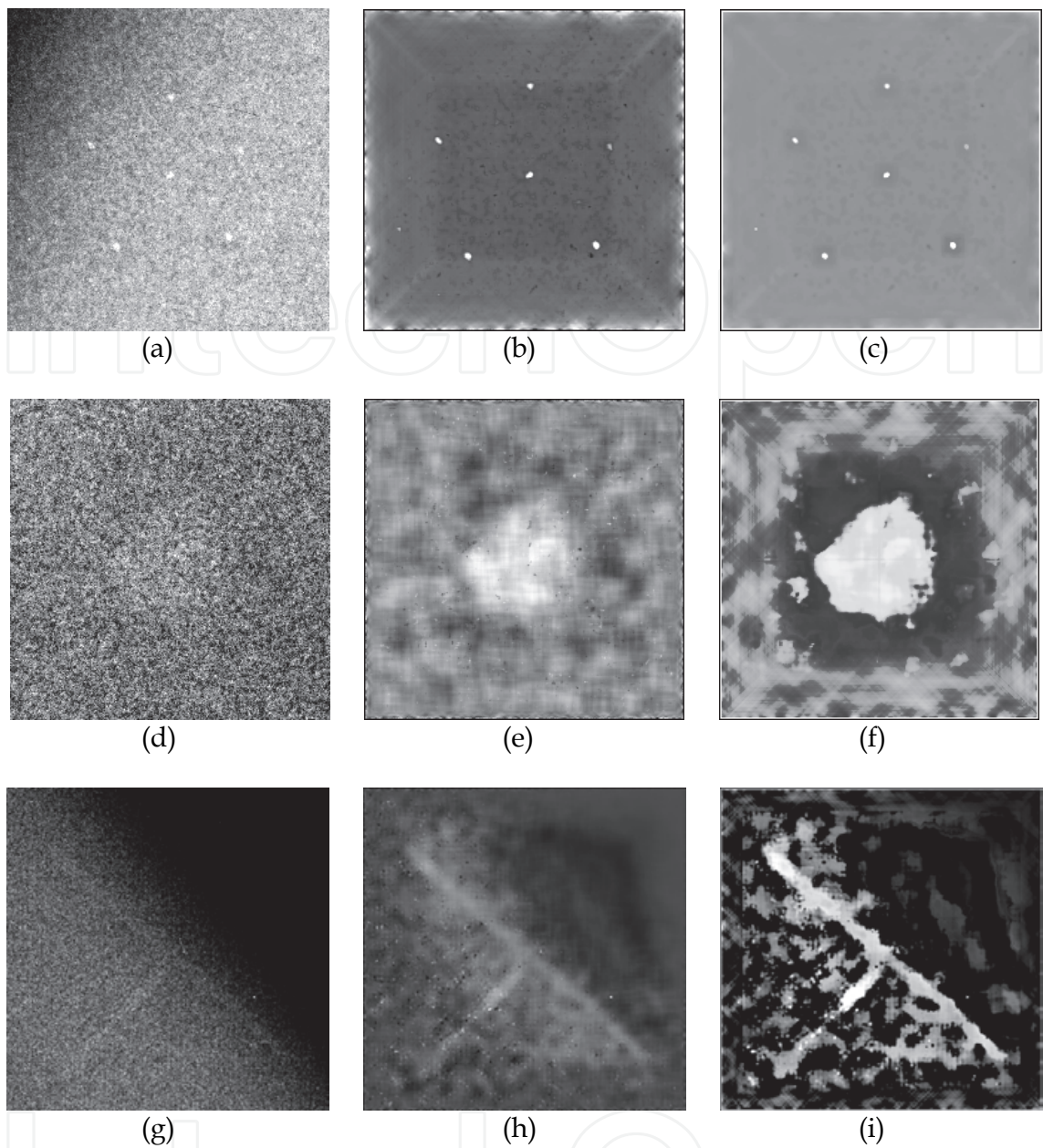


Fig. 6. Noise reduction and contrast enhancement steps on extracted subimages (a), (d) and (g): original extracted subimages; (b), (e) and (h) denoised images; (c), (f) and (i) contrast enhanced images.

4. Segmentation of extracted subimages

4.1 Microcalcification segmentation case

Microcalcifications segmentation was based on the computation of a cross-correlation between a template image  $M_{mic}$  and the preprocessed resulting image after noise reduction and contrast enhancement  $I_{net}$ . The different steps of microcalcification groups are summerized in figure 7. The template image was built after a supervised learning on real phantom images. A global thresholding was then applied on the thresholded image for extracting microcacifications. The connected component labelling step is done to determine the number of detected objects in  $I_{seuil}$  image. The microcalcification extraction step

consisted in defining around each detected object, a window centered on it and using a threshold based on the computation of the mean and standard deviation of pixels within this window. Fig 8 shows an example of microcalcifications group segmentation.

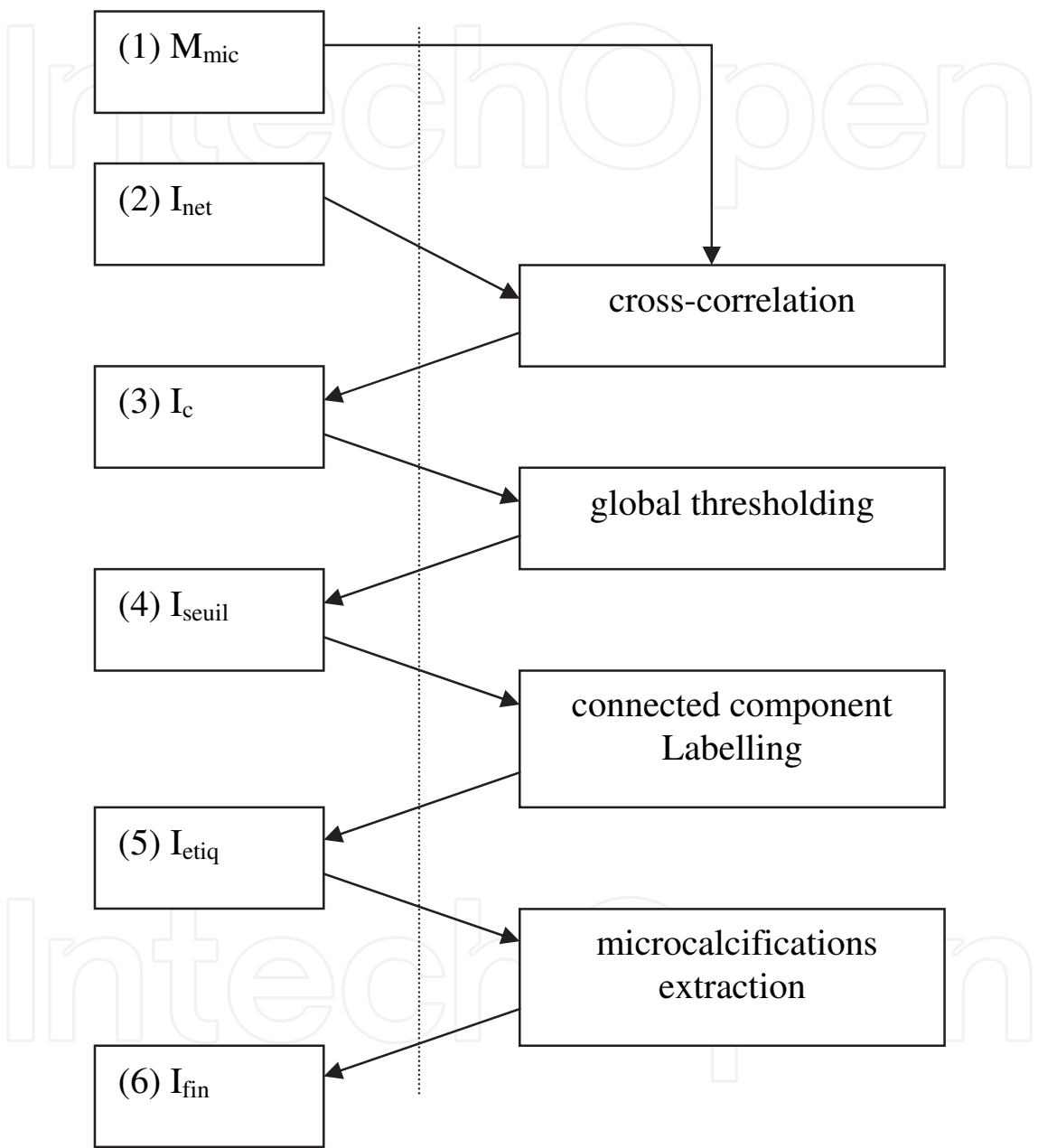


Fig. 7. General scheme of microcalcification group segmentation. (1)  $M_{mic}$  : template image, (2)  $I_{net}$  : resulting image after noise reduction and contrast enhancement, (3)  $I_c$  : resulting image after cross-correlation, (4)  $I_{seuil}$  : thresholded cross-correlated image, (5)  $I_{etiq}$  : connected component labelled image, (6)  $I_{fin}$  : resulting image with detected microcalcifications.

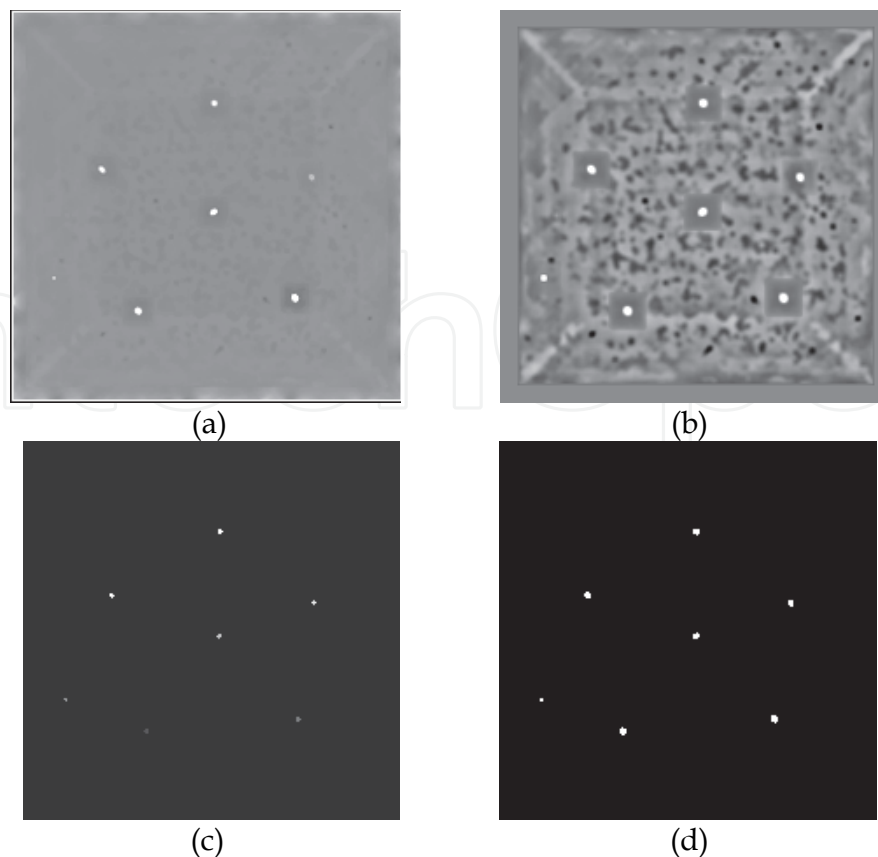


Fig. 8. Segmentation of microcalcifications. (a): extracted subimage after noise reduction and contrast enhancement  $I_{net}$  ; (b): result of template matching  $I_c$ ; (c): connected component labelled image  $I_{etiq}$  ; (d): resulting image  $I_{fin}$ .

#### 4.2 Mass segmentation case

Mass segmentation was done by using an active contour. First a square was set as an initial contour and the energy used depended only on image gradient. The algorithm used for that purpose is described as follows:

Step 1: Each point  $i$  of the active contour evolved along the normal of segment  $(i-1, i+1)$  until it met a mass edge.

Step 2: When the four initial points reached the mass edges, other points were added between each couple of points ( $i$  and  $i+1$ ).

Step 3: Each added point in the previous step evolved as initials points in step 1.

The algorithm stopped when a fixed but great number of iterations was reached. Fig. 9 shows an example of a mass segmentation.

#### 4.3 Fibre segmentation case

As for microcalcifications, fibre segmentation used a template matching between two template images (see Fig. 10) and the preprocessed resulting fibre image after applying noise reduction and contrast enhancement steps. An automatic global thresholding is then used, followed by a logical filter OR and a connected component labelling step. Figs. 11 and 12 show the general scheme of a fibre segmentation and an example of fibre segmentation respectively.

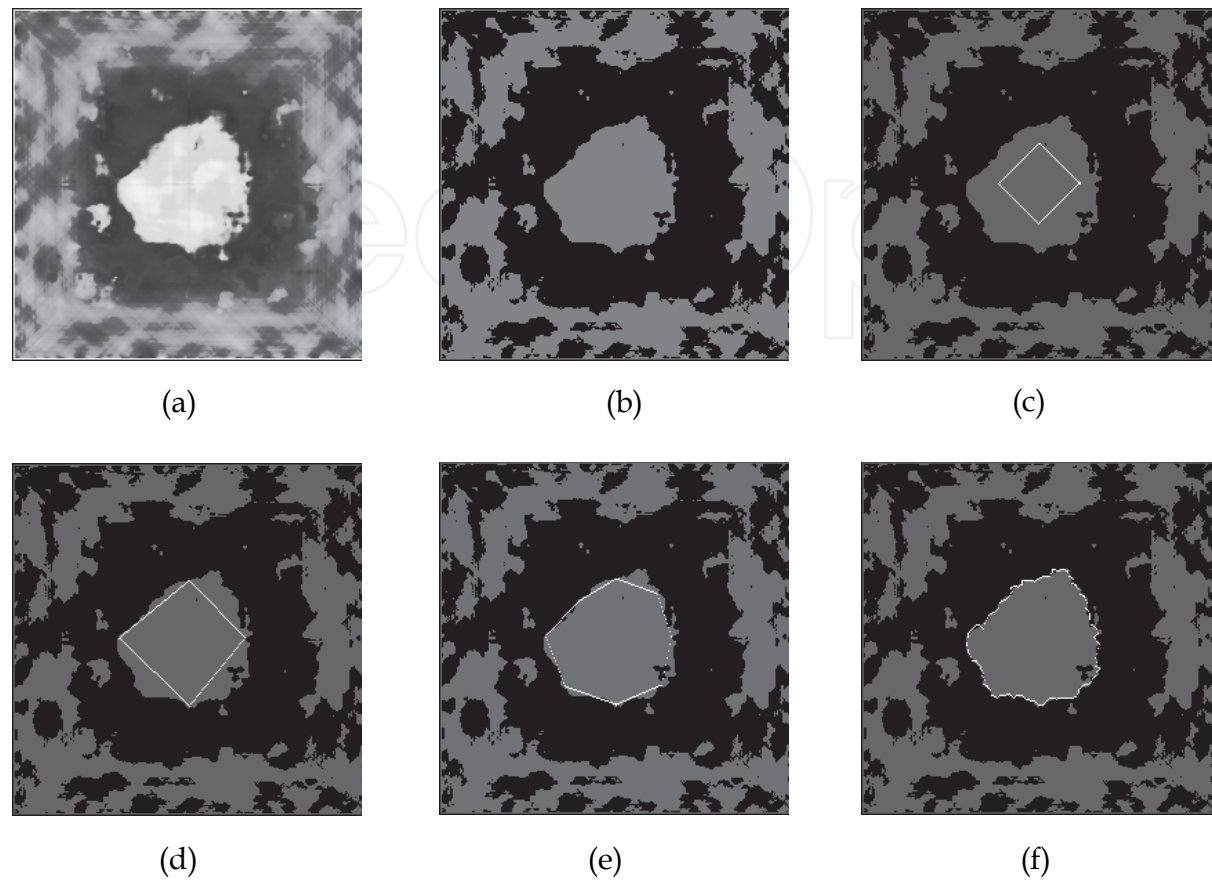


Fig. 9. Segmentation of a mass subimage (a): extracted subimage after noise reduction and contrast enhancement; (b): Thresholded image. (c): Initialization of active contour. (d) First iteration of the active contour. (e): Second iteration of active contour. (f): final segmentation.

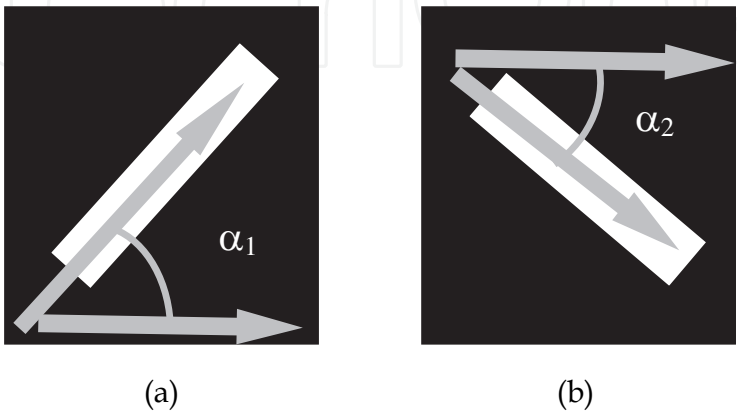


Fig. 10. Template images for fibre segmentation.



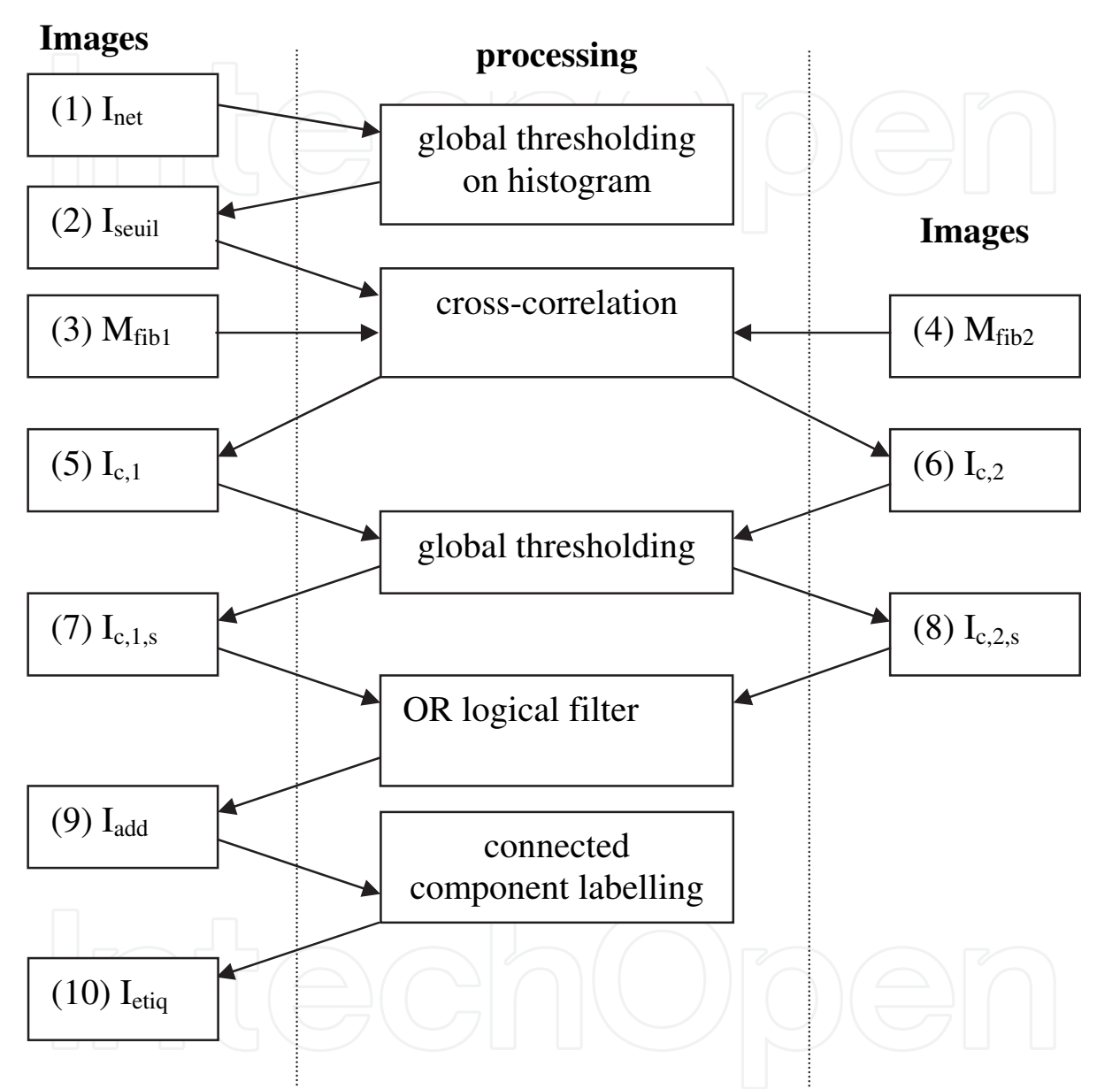


Fig. 11. General scheme of fibre segmentation. (1)  $I_{net}$  : resulting image after noise reduction and contrast enhancement , (2)  $I_{seuil}$  : image  $I_{net}$  thresholded , (3)  $M_{fib1}$  : template image 1, (4)  $M_{fib2}$  : template image 2, (5)  $I_{c,1}$  : obtained image after cross correlation between  $M_{fib1}$  and  $I_{seuil}$  , (6)  $I_{c,2}$  : obtained image after cross correlation between  $M_{fib2}$  and  $I_{seuil}$  (7)  $I_{c,1,s}$  : image  $I_{c,1}$  thresholded , (8)  $I_{c,2,s}$  : image  $I_{c,2}$  thresholded , (9)  $I_{add}$  : resulting image after logical filter OR between  $I_{c,1,s}$  and  $I_{c,2,s}$  (10)  $I_{etiq}$  : connected component labelled image.

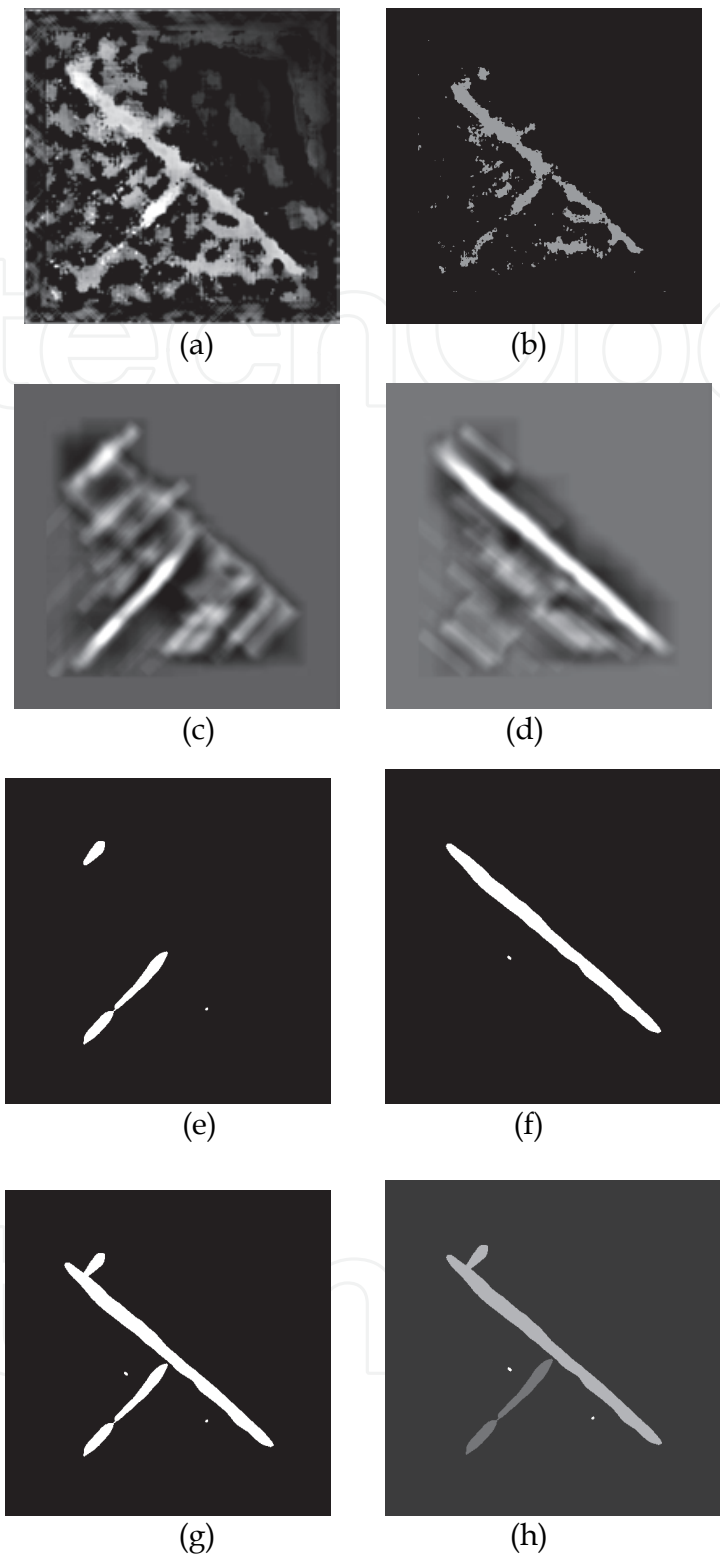


Fig. 12. Segmentation of a fibre subimage. (a): extracted subimage after noise reduction and contrast enhancement; (b): Thresholded image (c): Result of template matching with template image in Fig. 10(a); (d): Result of template matching with template image in Fig. 10(b); (e): Resulting image after thresholding image (c); (f): Resulting image after thresholding image (d); (g): Resulting image after applying OR logic filter on images (e) and (f); (h): Connect component labelled image.

5. Results and discussion

Nine phantom images from different mammographic facilities were tested. For each phantom image, only 4 subimages of each target were extracted. Two main reasons led us to do this choice: first, readers could not detect more than 4 objects on the phantoms used in our study, and second, a mammographic facility is considered to have good quality phantom films if at least 4 objects are detected from each embedded target.

216 microcalcifications (36 microcalcification groups) were studied. The most prominent microcalcification group M1 and M2 were almost all detected. Microcalcifications that were not detected were those with poor contrast. False detections were due to film emulsion tearing and appeared on M3 and M4 groups. Table 1 summarizes results obtained on these nine phantom films.

Thirty six masses and 36 fibres were studied. Three masses among 36 were not detected because of the non convergence of the iterative active contour algorithm. This appeared on masses containing holes when being preprocessed. When better initialising the active contour, it was possible to detect the whole masses.

The whole fibres were detected but as seen in Fig 12 some other objects appeared on the final segmentation image. These small objects will be removed in a further processing.

		1	2	3	4	5	6	7	8	9
M1 group	<i>Detected microcalcifications number</i>	6	6	6	6	6	6	6	6	6
	<i>False detection</i>									
M2 group	<i>Detected microcalcifications number</i>	6	6	6	6	6	6	6	6	6
	<i>False detection</i>	1					1		3	
M3 group	<i>Detected microcalcifications number</i>	6	6	6	6	5	6	5	6	5
	<i>False detection</i>	5	4	1	3	2				
M4 group	<i>Detected microcalcifications number</i>	6	6	6	6	3	6	5	4	6
	<i>False detection</i>	3	3	2			1			1

Table 1. Detection results on microcalcification groups.

## 6. Conclusion

This chapter presents a feasibility study of automating breast phantom scoring using image processing techniques. The main contribution in this project is noise reduction and contrast enhancement of noisy images extracted from digitized phantom films. The segmentation step which uses known methods shows that quality control in mammographic facilities could be done using image processing techniques. Next step in this project is to adapt image processing techniques used for digitized film to digital phantom images acquired directly from Full-Filed Digital Mammograms. In this case it will be possible to control the quality of digital mammographic systems using software similar to the one described in this study.

## 7. References

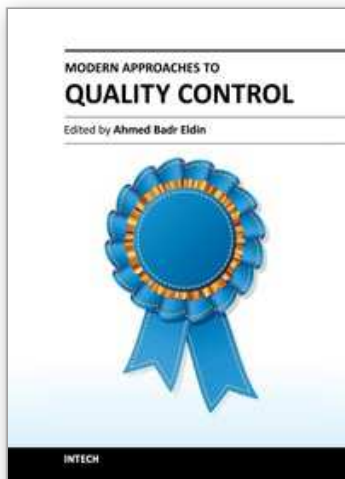
- K. W. Brooks, J. H. Trueblood, K. J. Kearfott, D. T. Lawton "Automated analysis of the American College of Radiology mammographic accreditation phantom images". Medical Physics 24 : 907-923, 1997.
- D. P. Chakraborty "Computer analysis of mammography phantom images (CAMPI). Application to the measurement of microcalcification image quality of directly acquired digital images". Medical Physics 24 : 1269-1277, 1997.
- G. Dougherty "Computerised evaluation of mammographic image quality using phantom images". Computerized Medical Imaging and Graphics 22: 365-373, 1998.
- A. D. Castellano Smith, I. A. Castellano Smith, D. R. Dance. "Objective assessment of phantom image quality in mammography: a feasibility study". The British Journal of Radiology 71 : 48-58, 1998
- L. Blot, A. Davis, M. Holubinka ,R. Marti, R. Zwiggelaar "Automated quality assurance applied to mammographic imaging". EURASIP Journal on Applied Signal Processing 7 : 736-745, 2003
- P. Mayo, F. Rodenas, G. Verdu, J. I. Villaescusa, J. M. Campayo. "Automatic evaluation of the image quality of a mammographic phantom". Computers Methods and Programs in Biomedicine 73, 115-128, 2004
- A. P. Dhawan, G. Buelloni R. Gordon, "Enhancement of mammographic features by optimal adaptative neighborhood image processing," IEEE Trans. Medical Imaging 5(1), 8-15, 1986.
- A. P. Dhawan E. Le Royer "Mammographic feature enhancement by computerized image processing". Computer Methods and Programs in Biomedicine 27, 23-25, 1988.
- V. Guis, M. Adel, M. Rasigni, G. Rasigni, B. Seradour, P. Heid "Adaptive neighborhood contrast enhancement in mammographic phantom images". Optical Engineering 42: 357-366, 2003.
- W. Qian, L.P. Clarke, M. Kallergi, R. A. Clark, "Tree-Structured Nonlinear Filters in Digital Mammography". IEEE Trans. Medical Imaging 13(1), 25-36, 1994.
- F. Aghadasi, R. K. Ward, B. Palcic, "Noise filtering for mammographic images", *14<sup>th</sup> Annual International Conference of the I.E.E.E. Engineering in Medicine and Biology Society* 1877-1878, 1992.



- D. T. Kuan, A. A. Shawchuk, T. C. Strand, P. Chavel, "Adaptive noise smoothing filter for images with signal-dependent noise". IEEE Trans. Patt. Anal. Mach. Intell. 7(2), 165-177, 1985.

IntechOpen

IntechOpen



## **Modern Approaches To Quality Control**

Edited by Dr. Ahmed Badr Eldin

ISBN 978-953-307-971-4

Hard cover, 538 pages

**Publisher** InTech

**Published online** 09, November, 2011

**Published in print edition** November, 2011

Rapid advance have been made in the last decade in the quality control procedures and techniques, most of the existing books try to cover specific techniques with all of their details. The aim of this book is to demonstrate quality control processes in a variety of areas, ranging from pharmaceutical and medical fields to construction engineering and data quality. A wide range of techniques and procedures have been covered.

### **How to reference**

In order to correctly reference this scholarly work, feel free to copy and paste the following:

Mouloud Adel and Monique Rasigni (2011). Mammographic Quality Control Using Digital Image Processing Techniques, Modern Approaches To Quality Control, Dr. Ahmed Badr Eldin (Ed.), ISBN: 978-953-307-971-4, InTech, Available from: <http://www.intechopen.com/books/modern-approaches-to-quality-control/mammographic-quality-control-using-digital-image-processing-techniques>

**INTECH**  
open science | open minds

### **InTech Europe**

University Campus STeP Ri  
Slavka Krautzeka 83/A  
51000 Rijeka, Croatia  
Phone: +385 (51) 770 447  
Fax: +385 (51) 686 166  
[www.intechopen.com](http://www.intechopen.com)

### **InTech China**

Unit 405, Office Block, Hotel Equatorial Shanghai  
No.65, Yan An Road (West), Shanghai, 200040, China  
中国上海市延安西路65号上海国际贵都大饭店办公楼405单元  
Phone: +86-21-62489820  
Fax: +86-21-62489821

© 2011 The Author(s). Licensee IntechOpen. This is an open access article distributed under the terms of the [Creative Commons Attribution 3.0 License](https://creativecommons.org/licenses/by/3.0/), which permits unrestricted use, distribution, and reproduction in any medium, provided the original work is properly cited.

IntechOpen

IntechOpen